Effects of CO_2 geosequestration on opalinus clay.

ASIM, T. and HAWEZ, H.K.

2024

energies

MDPI

Article

Effects of CO_2 Geosequestration on Opalinus Clay

Taimoor Asim [1,*] and Haval Kukha Hawez [1,2]

[1] School of Engineering, Robert Gordon University, Aberdeen AB10 7GJ, UK
[2] Department of Petroleum Engineering, Faculty of Engineering, Koya University, Koya KOY45, Kurdistan Region–F.R., Iraq
* Correspondence: t.asim@rgu.ac.uk

Abstract: CO_2 geosequestration is an important contributor to United Nations Sustainable Development Goal 13, i.e., Climate Action, which states a global Net-Zero CO_2 emissions by 2050. A potential impact of CO_2 geosequestration in depleted oil and gas reservoirs is the variations in induced pressure across the caprocks, which can lead to significant local variations in CO_2 saturation. A detailed understanding of the relationship between the pressure gradient across the caprock and local CO_2 concentration is of utmost importance for assessing the potential of CO_2 geosequestration. Achieving this through experimental techniques is extremely difficult, and thus, we employ a coupled Computational Fluid Dynamics (CFD) and Finite Element Method (FEM) based solver to mimic sub-critical CO_2 injection in Opalinus Clay under various pressure gradients across the sample. The geomechanical and multiphase flow modelling utilising Darcy Law helps evaluate local variations in CO_2 concentration in Opalinus Clay. Well-validated numerical results indicate favourable sub-critical CO_2 geosequestration under a positive pressure gradient across Opalinus Clay. In the absence of a positive pressure gradient, a peak CO_2 concentration of 5% has been recorded, which increases substantially (above 90%) as the pressure gradient across the sample increases.

Keywords: Opalinus Clay; Computational Fluid Dynamics; Finite Element Analysis; CO_2 geosequestration

Citation: Asim, T.; Hawez, H.K. Effects of CO_2 Geosequestration on Opalinus Clay. *Energies* **2024**, *17*, 2431. https://doi.org/10.3390/en17102431

Academic Editor: Alberto Pettinau

Received: 8 April 2024
Revised: 14 May 2024
Accepted: 16 May 2024
Published: 19 May 2024

1. Introduction

Carbon capture and storage (CCS) has become a viable technology in the search for sustainable energy solutions and the reduction of anthropogenic greenhouse gas emissions. The main component of CCS is the injection of CO_2 into deep geological formations, where it may be safely stored for geologically long periods. These formations often consist of salty aquifers or depleted oil and gas reservoirs. The behaviour of subsurface formations, particularly the caprock, which serves as a primary seal to inhibit the upward migration of injected CO_2, is crucial to the effectiveness and safety of CCS. Shale formations are among the most popular options for caprock materials due to their low permeability and widespread occurrence. However, little is known about the hydromechanical response of shale caprocks to CO_2 injection [1]. Shale formations are often chosen as caprocks for CO_2 storage reservoirs due to their fine-grained structure and low permeability [2]. To ensure the long-term containment of injected CO_2, these caprocks must remain intact. Therefore, it is essential to understand how shale caprocks react to CO_2 injection to assess the security and feasibility of CCS operations [3,4]. The hydromechanical response of shale caprocks to CO_2 injection involves a complex interplay of fluid flow and geomechanical deformation [5,6]. The injection of CO_2 alters the shale's pore pressure and fluid content, thereby affecting its mechanical characteristics [7]. These interconnected processes have the potential to impact caprock structural integrity and CO_2 confinement [8,9].

The hydromechanical reaction of shale caprocks to CO_2 injection can effectively be modelled and analysed using numerical methods [10]. Finite Element Method (FEM) is often employed to evaluate the mechanical integrity of reservoir rocks and caprocks under

the stresses induced by CO_2 injection [11]. It aids in predicting probable deformation, fractures, and important elements in guaranteeing the long-term containment of CO_2. The assessment of CO_2 saturation and hydromechanical response has been studied extensively using Computational Fluid Dynamics (CFD) to model fluid flow within reservoirs and surrounding formations, accounting for factors such as porosity, permeability, and fluid properties [12,13]. Moreover, CFD is used for evaluating risks involved with the dispersion of CO_2 in the atmosphere as a result of leakage, leading to its high-velocity release [14]. Such studies provide accurate predictions of gas phase transportation and help evaluate the risks involved in CCS projects. In order to describe the complex behaviour of shale caprocks when CO_2 is injected into them, the numerical models can accurately predict the multiphase flow mechanisms and complex constitutive linkages [15,16]. While significant progress has been made in the accuracy of numerical predictions, numerous unknowns and challenges persist in predicting the hydromechanical response of shale caprocks to CO_2 injection [17,18]. These include validating the numerically predicted results against laboratory and field tests, accurately representing shale variability, understanding fluid-rock interactions, and addressing coupled processes at various spatial and temporal scales.

Apart from validating the numerical models, another important factor is the assessment of CO_2 geosequestration in shale caprocks like Opalinus Clay. This requires local measurements of CO_2 concentration within the caprock, which is not easily achievable using experimental techniques. Numerical modelling, however, can be used to evaluate local CO_2 concentration in caprocks. Resolving this critical issue is crucial for enhancing our understanding of shale caprock behaviour for CO_2 storage and improving the predictive capability of numerical models [19]. The design, management, and risk assessment of CCS projects are significantly impacted by these findings, which also influence methods to maintain the integrity and efficacy of CO_2 storage in shale formations over the long term [20,21].

Regional pressure variations play a significant role in dictating CO_2 geosequestration in geological formations [22,23]. The extent of CO_2 geosequestration significantly impacts how much CO_2 can be stored in shale caprocks. However, published literature is severely lacking in analysing this important aspect of CO_2 geosequestration. Thus, we aim to bridge this gap in scientific knowledge through numerical modelling. A coupled CFD-FEM model utilizing Darcy's Law is employed to better understand the complex dynamics of local variations in CO_2 concentration in shale caprock Opalinus Clay, which is the primary aim of this investigation. It is envisaged that through the results obtained through this investigation, well-informed decisions can be made in future while planning CCS projects and evaluating their technical feasibility and economic viability.

2. CFD-FEM Model

A coupled CFD-FEM model has been utilized to model the complex geomechanical and multiphase flow behaviour of sub-critical CO_2 injection in a water-saturated sample of Opalinus Clay. As there are two phases involved in the numerical model, i.e., water and CO_2, where CO_2 injection leads to water displacement in the sample, their mass balance is modelled as follows:

$$\frac{\partial}{\partial t}\left(\varphi S_\beta \rho_\beta\right) - \nabla\cdot\left(\rho_\beta u_\beta\right) - \Psi_\beta = 0 \quad (1)$$

where β represents a phase, φ is porosity, S is saturation, ρ is density, u is Darcy velocity, and Ψ is the source term. The Darcy velocity (u) can be expressed as:

$$u_\beta = -\frac{k_a Kr_\beta}{\mu_\beta}\nabla P_\beta \quad (2)$$

where k_a is absolute permeability, K_r is relative permeability, and P is pore pressure. The source term (Ψ) in Equation (1) can be defined as:

$$\Psi_\beta = \rho_\beta \alpha_B \left(\frac{\partial \varepsilon_{vol}}{\partial t} \right) \tag{3}$$

here, α is the Biot coefficient and ε_{vol} is volumetric strain, which is modelled as:

$$\varepsilon_{vol} = \frac{1}{2}\left[(\nabla d)^2 + \nabla d \right] \varepsilon_{ij} = \frac{1}{2}\left(\frac{\partial d_i}{\partial x_j} + \frac{\partial d_j}{\partial x_i} \right) \tag{4}$$

where d is the displacement of the sample. The effects of gravity are ignored, and thus, the pressure gradient acts as the only driving force for the transport of CO_2 within the sample. The relationship between the Biot coefficient (α) in Equation (3) and Biot Modulus (M) is:

$$\frac{1}{M} = \frac{\varphi}{K_d} + \frac{\alpha_B - \varphi}{K_s} \tag{5}$$

where K_d is the drained bulk modulus and K_s is the solid bulk modulus. Moreover:

$$\frac{\partial}{\partial t}\left(\varphi S_\beta \rho_\beta \right) = \frac{1}{M} \frac{\partial \left(S_\beta \rho_\beta p_\beta \right)}{\partial t} \tag{6}$$

Now, the governing mass conservation equation can be obtained for the fully coupled numerical model as:

$$\left(\frac{\varphi}{K_d} + \frac{\alpha_B - \varphi}{K_s} \right) \frac{\partial \left(S_\beta \rho_\beta p_\beta \right)}{\partial t} - \nabla \cdot \left(\frac{k_a Kr_\beta \rho_\beta}{\mu_\beta} \nabla P_\beta \right) = \rho_\beta \alpha_B \left(\frac{\partial \varepsilon_{vol}}{\partial t} \right) \tag{7}$$

The force equilibrium (or solid deformation) can be represented as:

$$\nabla \cdot \sigma + \left(\rho_\beta \varphi + \rho_\beta \right) g = 0 \tag{8}$$

$$\sigma = \sigma' - \alpha_B P_\beta I \tag{9}$$

where σ and σ' are total and effective stress, respectively, and I is the second-order identity tensor. The porosity (φ) is dependent on the elastic modulus (E) as [24]:

$$\ln\left(\frac{E}{E_i} \right) = -d(\varphi_i - \varphi) \tag{10}$$

As the caprock sample undergoes compression, the ability of multiphase flow through it changes. Thus, the permeability (k) can be modelled as [25]:

$$k = k_i \left\{ 1 \pm \frac{1}{2} \left[\frac{9(1-\nu^2)}{2} \left(\frac{\pi \Delta \sigma}{E} \right)^2 \right]^{1/3} \right\}^2 \tag{11}$$

where k_i is the initial matrix permeability. The positive sign refers to dilatational loading, while the negative sign corresponds to compression loading.

The effective viscosity (μ_{eff}) is modelled as:

$$\mu_{eff} = \frac{\rho_{total}}{\frac{K_{rw}\rho_w}{\mu_w} - \frac{K_{rg}\rho_g}{\mu_g}} \tag{12}$$

while the total density is represented as:

$$\rho_{total} = S_w \rho_w + S_g \rho_g \quad (13)$$

The Brooks and Corey model [26] has been utilized to find out the saturation of each phase in the caprock as:

$$S_g = \frac{(S_{ig} - S_{rg})}{(1 - S_{rg} - S_{rw})} \quad (14)$$

$$S_w = \frac{(S_{iw} - S_{rw})}{(1 - S_{rg} - S_{rw})} \quad (15)$$

where the subscripts i, r, w, g represent initial, residual, water, and gas (CO_2), respectively.

3. Methods and Materials

3.1. Opalinus Clay Model and Properties

The Opalinus Clay caprock has been modelled as a 35 mm × 12 mm two-dimensional (2D) rectangular flow domain having a bulk density of 2.75 g/cm^3, as considered by Minardi et al. [27]. 2D geometric modelling of Opalinus Clay is appropriate given the expected laminar flow in the domain and the absence of Reynolds stresses. Moreover, 2D modelling significantly reduces the computational cost provided that the model is well-validated against experimental data. The different properties of the Opalinus Clay model are summarized in Table 1.

Table 1. Properties of Opalinus Clay model [27].

Property	Value
Initial Porosity	0.1 [-]
Initial Permeability	2.4×10^{-20} [m^2]
Young Modulus	6 [GPa]
Poisson ratio	0.25 [-]
Initial Pore Pressure	1 [atm]
Entry capillary pressure	5 [Pa]
Pore size distribution index	0.67 [-]
Biot-Willis coefficient	0.76 [-]

3.2. Meshing of the Flow Domain

The numerical work builds upon the experimental findings of Minardi et al. [27] and posits that CO_2 is injected into the model under different pressure gradients across the Opalinus Clay model. This injection pressure is countered by water pressure acting in the opposite direction to offset the impact of CO_2 injection. Thus, CO_2 displaces water in the model. To assess CO_2 saturation response, the flow domain has been spatially discretised, as illustrated in Figure 1. The mesh shown here comprises 0.9×10^4 structured elements.

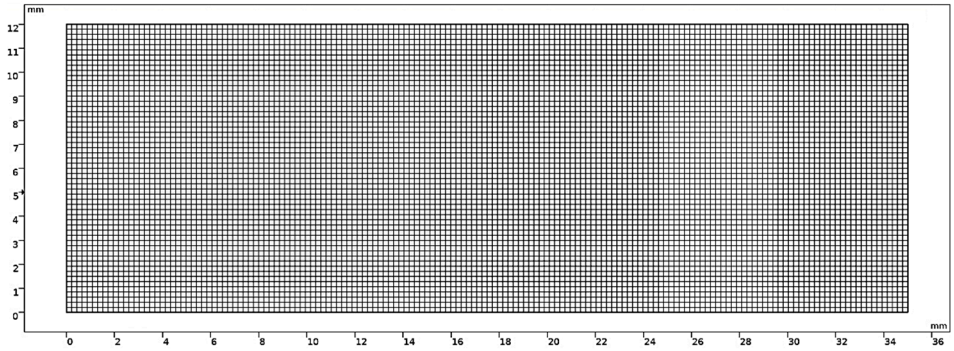

Figure 1. The meshing of the flow domain.

To ensure the numerical predictions are robust and independent of mesh sizing used [10], four additional meshes are generated, comprising 0.5×10^4, 0.6×10^4, 0.75×10^4 and 2×10^4 elements. All the meshes generated are analysed for sample displacement (d), a key parameter later used to validate our numerical model against the experimental data [27]. The results of the mesh independence tests are depicted in Figure 2. Notably, as the number of elements increased from 0.5×10^4 to 0.9×10^4, the displacement also increased. However, the difference in displacement between 0.9×10^4 and 2×10^4 elements was negligible. Consequently, the mesh with 0.9×10^4 elements, shown in Figure 1, has been selected for further analysis.

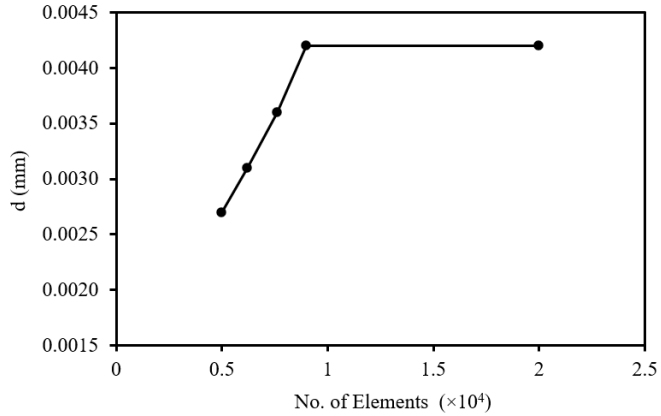

Figure 2. Mesh independence test results.

3.3. Scope of Work

As this investigation evaluates the potential of sub-critical CO_2 geosequestration in Opalinus Clay, the maximum injection pressure of CO_2 is limited to 8 MPa [27]. Extensive numerical investigations have been carried out under two specific conditions, i.e., no pressure gradient across the Opalinus Clay sample and a positive pressure gradient.

$$P_{in} - P_{out} = \begin{cases} = 0 \text{ no pressure gradient} \\ > 0 \text{ positive presure gradient} \end{cases}$$

where P_{in} is CO_2 injection pressure (limited to 8 MPa), and P_{out} is the pressure at the outlet of the model. For no pressure gradient condition, P_{in} and P_{out} remain the same, while for positive pressure gradient, $P_{in} > P_{out}$. The complete scope of the work is presented in Table 2.

Table 2. Scope of the numerical modelling.

P_{in} (MPa)	P_{out} (MPa)	Pressure Gradient
1	1	No
	0	Yes
2	2	No
	1	Yes
	0	Yes
4	4	No
	2	Yes
	0	Yes

Table 2. *Cont.*

P_{in} (MPa)	P_{out} (MPa)	Pressure Gradient
8	8	No
	6	Yes
	4	Yes
	2	Yes
	0	Yes

3.4. Numerical Model Setup

COMSOL Multiphysics 6.1 has been used to analyse two-phase fluid flow in Opalinus Clay, which has been modelled as porous media, incorporating geomechanics. Both the poroelastic module (which couples Darcy's law with solid mechanics) and multiphase modules (which couples Darcy's law with phase transportation) are utilized. The numerical model's execution involves updating porosity values based on generated strain in the caprock following convergence at each time step. An adaptive time-stepping method has been used, which automatically adjusts the actual time step size in order to achieve solver convergence. CO_2 injection total time is 48 h and is based on the experimental work of Minardi et al. [27].

The updated porosity values are used to determine spatially varying elastic modulus. The Opalinus Clay model's permeability is defined as a function of volumetric strain. Updated values are iteratively returned to the property definition after each time step ($t + \Delta t$). The PARADISO (Parallel Direct Solver) with a pivoting perturbation of 10^{-8} is utilized to solve the nonlinear system of equations in conjunction with the Newton nonlinear method.

4. Results and Discussion

This section presents the results obtained from the numerical investigations, highlighting the role of pressure gradient across Opalinus Clay in CO_2 geosequestration. The primary multiphase flow parameter that has been analysed is the concentration of CO_2 in Opalinus Clay, as it clearly demonstrates the potential of CO_2 sequestration in geological formations, which cannot be easily measured through experimental procedures.

4.1. Validation of the Numerical Model

In order to gain confidence in the numerical results obtained, the numerical model has been validated against the experimental data. Minardi et al. [27] experimentally studied the injection of sub-critical CO_2 in the Opalinus Clay core sample at different injection and outlet pressures, summarised in Table 3, and measured the core sample's vertical displacement (d). The scope of work includes the conditions considered by Minardi et al. [27]. It can be clearly seen that the numerically predicted vertical displacement of the Opalinus Clay model matches accurately with experimentally measured vertical displacement of the core sample (maximum difference of 5%), clearly demonstrating the efficacy of the developed numerical model to be used for other pressure gradient conditions summarized in Table 2.

Table 3. Comparison of numerical and experimental vertical displacement of Opalinus Clay sample.

P_{in} (MPa)	P_{out} (MPa)	$d_{experimental}$ (mm)	$d_{numerical}$ (mm)	Difference (%)
2	2	0.004	0.0042	+5.0
4	2	0.007	0.0068	+2.8

4.2. CO_2 Saturation under No Pressure Gradient

This section provides detailed qualitative and quantitative analyses of the numerical results obtained for no pressure gradient across the Opalinus Clay sample, corresponding to the Pressure Gradient [No] in Table 2. Thus, this section's CO_2 injection and outlet pressures remain the same. Figure 3 depicts CO_2 saturation in the Opalinus Clay sample for the different injection pressures considered, i.e., 1 MPa, 2 MPa, 4 MPA, and 8 MPa. It can be clearly seen that as CO_2 is injected into the sample, despite no pressure difference between the inlet and outlet boundaries of the sample, CO_2 concentration increases in the vicinity of the inlet boundary of Opalinus Clay. Increasing CO_2 injection pressure further saturates the clay sample from the inlet boundary side, i.e., CO_2 penetrates the inlet boundary further downstream and gets stored in the sample. The scale in Figure 3 has been kept constant (0% to 10% concentration) for the different injection pressure values for effective comparison purposes. Interestingly, even when CO_2 injection pressure increases eightfold (between Figure 3a,d), the peak CO_2 concentration value doesn't change noticeably, a phenomenon that needs further investigation.

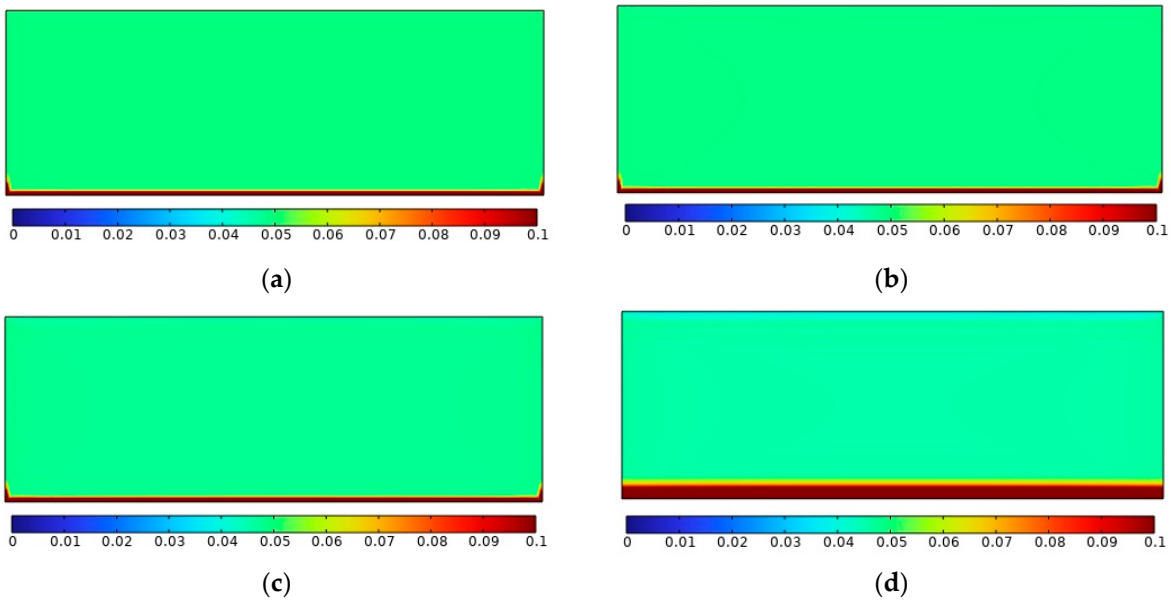

Figure 3. Spatial variations in CO_2 concentration under no pressure gradient and injection pressures of (**a**) 1 MPa (**b**) 2 MPa (**c**) 4 MPa (**d**) 8 MPa.

Figure 4 depicts CO_2 concentration profiles in the axial direction of the Opalinus Clay model under no pressure gradient and for different injection pressures considered. The *Y*-axis shows the length of the sample while the *X*-axis shows CO_2 concentration, the scale of which has been zoomed in to show concentration variations from 4% to 6% only. It can be seen that at a CO_2 injection pressure of 1 MPa, its concentration is very high (100%) until $y/Y < 0.05$. This is potentially due to the boundary condition in the numerical solver. At $y/Y = 0.05$, a CO_2 concentration of 5% has been recorded, which then remains the same throughout the clay sample. Increasing CO_2 injection pressure to 2 MPa and 4 MPa decreases CO_2 concentration to 4.9% and 4.8%, respectively, throughout the sample; however, no significant change occurs near the inlet boundary, i.e., these concentration values are obtained at $y/Y = 0.05$. As the injection pressure increases to 8 MPa, which is very close to CO_2's critical pressure, we observe three significant changes. Firstly, at $y/Y = 0.05$, a CO_2 concentration of 12% is recorded, which eventually drops to 5% at $y/Y = 0.1$. Thus, CO_2 is injected deeper into the clay sample at this injection pressure. Secondly, between $0.1 < y/Y < 0.95$, a constant CO_2 concentration of 4.5% is recorded. When the injection pressure increased from 1 MPa to 2 MPa, this concentration decreased by 2%. When the injection pressure increased from 2 MPa to 4 MPa, this concentration

further decreased by 2%. When the injection pressure increased from 4 MPa to 8 MPa (still two folds increase), this concentration decreased by 6.25%. Thus, although near-inlet CO_2 concentration has more than doubled, inner sample concentration has decreased.

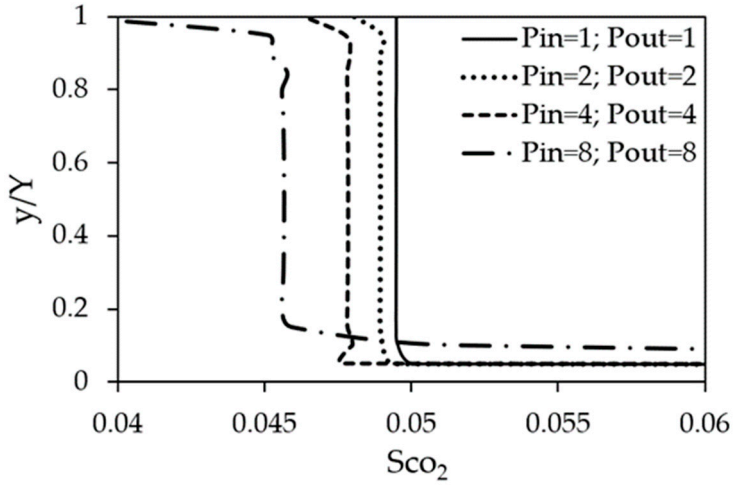

Figure 4. CO_2 concentration profiles in Opalinus Clay at different injection pressures under no pressure gradient.

Lastly, it can be observed that CO_2 concentration drastically decreases (to 3.9%) near the outlet boundary of the numerical model. As this has not been observed in the case of injection pressure of 1 MPa, and some minor decrease is observed at 2 MPa and 4 MPa, it is anticipated that this phenomenon is not due to the boundary condition at the outlet boundary of the model, rather seems influenced by the operating pressure of the sample. In conclusion, the potential of sub-critical CO_2 geosequestration in Opalinus Clay is severely limited and is not the preferred method.

4.3. CO_2 Saturation under Positive Pressure Gradient

This section presents the numerical results obtained under positive pressure gradient conditions when the outlet pressure is kept constant at 0 MPa (gauge). Figure 5 depicts spatial variations in CO_2 concentration at different injection pressures considered. The scale of these variations has been fixed to 84% to 100% based on the results obtained. As observed in the case of no pressure gradient cases, CO_2 concentration increases from the inlet boundary side; the same is observed in the case of the positive pressure gradient. However, contrary to no pressure gradient, significantly higher CO_2 concentration and considerable axial variations are observed. It can be seen in the figure that as the injection pressure increases, and consequently the pressure gradient, CO_2 concentration increases significantly in the Opalinus Clay model, clearly demonstrating favourable CO_2 sequestration in Opalinus Clay when subjected to the positive pressure gradient. A sudden positive jump in CO_2 concentration at the outlet boundary is visible and is attributed to the operating pressure, which needs further analysis.

Figure 6 depicts the axial CO_2 concentration profiles in the Opalinus Clay model at different injection pressures while the outlet pressure is kept constant at 0 MPa. At $y/Y = 0$ (inlet boundary), the concentration of CO_2 is 100%, irrespective of the pressure gradient. Moving axially downstream, CO_2 concentration drops, but this drop is dependent on the pressure gradient. As the pressure gradient increases, this drop in CO_2 concentration also decreases; thus, a higher pressure gradient leads to higher CO_2 storage in Opalinus Clay. Contrary to no pressure gradient cases, the axial CO_2 concentration profiles do not remain constant till the outlet boundary. Rather, the curves are (somewhat) C-shaped, i.e., CO_2 concentration, moving downstream from the inlet boundary, keeps decreasing till $y/Y = 0.7$ before increasing again till the outlet boundary (i.e., $y/Y = 1.0$). CO_2 concentration recovery of almost 5% is recorded for all the cases under consideration. In conclusion, a higher

pressure gradient leads to higher CO_2 concentration in Opalinus Clay, facilitating CO_2 geosequestration.

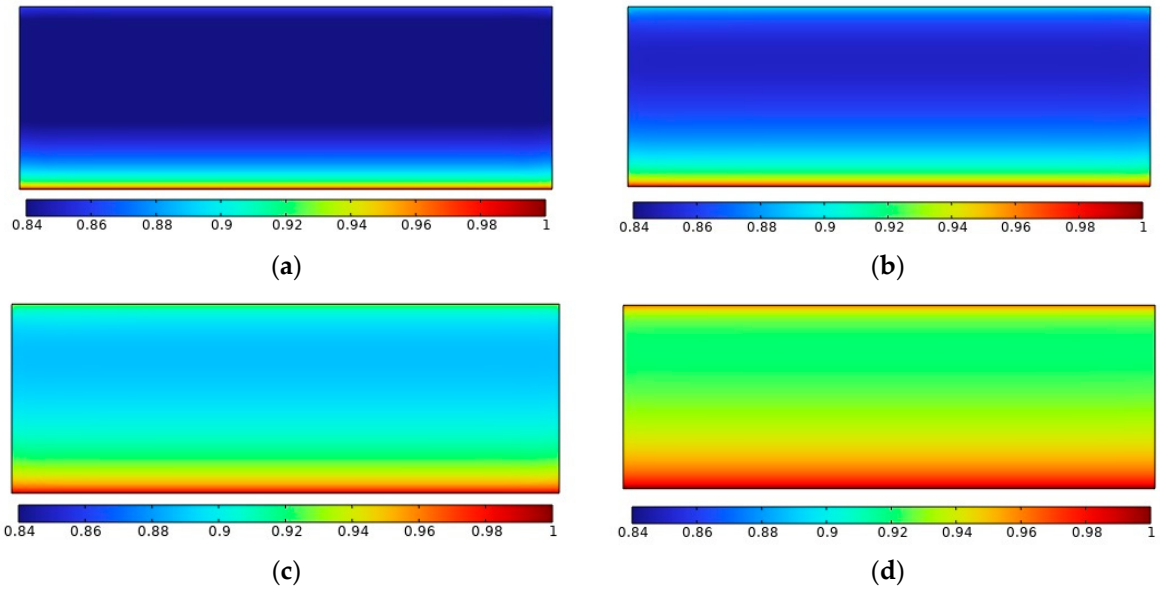

Figure 5. Spatial variations in CO_2 concentration under positive pressure gradient and injection pressures of (**a**) 1 MPa; (**b**) 2 MPa; (**c**) 4 MPa; (**d**) 8 MPa.

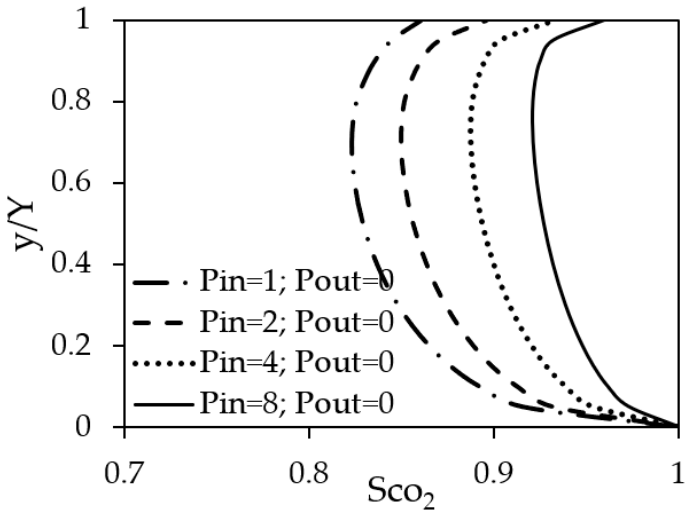

Figure 6. CO_2 concentration profiles in Opalinus Clay at different injection pressures under a positive pressure gradient.

4.4. Effects of Outlet Pressure on CO_2 Saturation

In the previous section, a positive pressure gradient was considered based on increasing injection pressure (P_{in}), while the outlet pressure (P_{out}) was kept constant at 0 MPa. In order to understand the impact of outlet pressure on CO_2 geosequestration, this section presents detailed analyses of the effects of increasing the outlet pressure on CO_2 concentration in the Opalinus Clay model. Figure 7 depicts the difference in CO_2 concentration in the Opalinus Clay model with respect to lower pressure gradient/s; thus, Figure 7a is basically the CO_2 concentration contour at (P_{in} = 2; P_{out} = 1) minus CO_2 concentration contour obtained for (P_{in} = 2; P_{out} = 2), while Figure 7b corresponds to (P_{in} = 2; P_{out} = 0) minus (P_{in} = 2; P_{out} = 1). Hence, Figure 7a depicts the difference in CO_2 concentration between a low positive pressure gradient and no pressure gradient, while Figure 7b depicts the difference between a high positive pressure gradient and a low positive pressure gradient.

Expectedly (from earlier results), as a pressure gradient (of 1 MPa) is introduced across the Opalinus Clay model, CO_2 concentration shoots up, and thus we see very large difference values (mostly brown). In comparison, when the pressure gradient rises further by 1 MPa, CO_2 concentration increases further; however, the difference is not as high as observed in Figure 7a. This further highlights the impact of pressure gradient on CO_2 storage in Opalinus Clay. The same is observed for P_{in} of 4 MPa however, as the injection pressure doubles, the penetration of CO_2 is observed further downstream the inlet boundary (as seen in Figure 7c). Meanwhile, very interestingly, increasing the pressure gradient leads to lesser changes near the inlet boundary. This is because CO_2 has already reached a very high concentration level in the near-inlet zone (as depicted in Figure 6), and thus, there is less margin for further enhancing CO_2 concentration in the near-inlet region. Following this explanation, it can be seen that in Figure 7e–h, the increase in CO_2 concentration slows down till we observe in Figure 7h that the increase in CO_2 concentration is only marginal. Thus, we conclude that knowing the injection pressure of CO_2 alone is not enough to predict CO_2 concentration in Opalinus Clay and that outlet pressure plays a significant role in dictating the extent of CO_2 geosequestration.

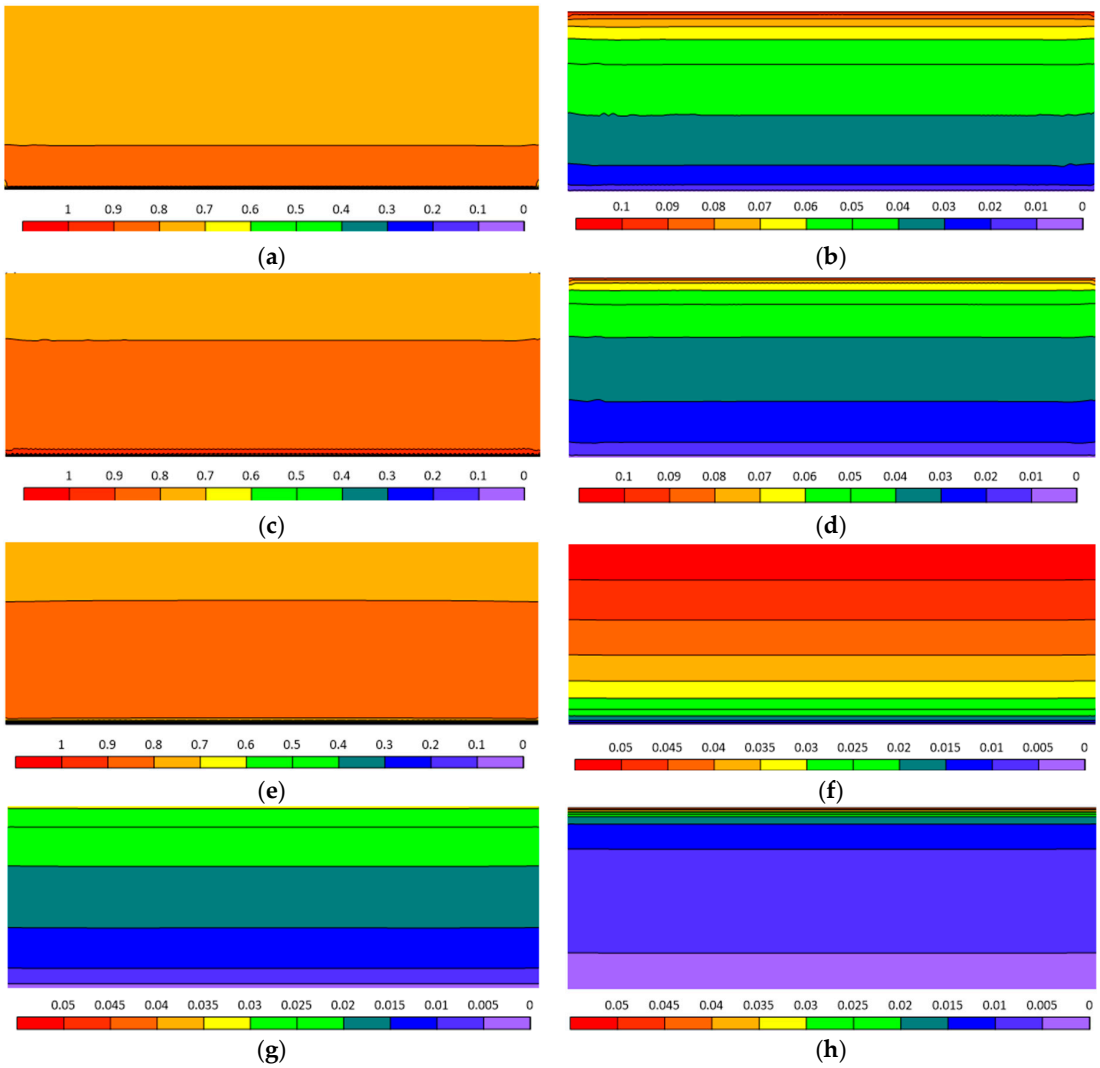

Figure 7. Differences in CO_2 concentration between successive levels of pressure gradient. (**a**) (P_{in} = 2; P_{out} = 1) − (P_{in} = 2; P_{out} = 2); (**b**) (P_{in} = 2; P_{out} = 0) − (P_{in} = 2; P_{out} = 1); (**c**) (P_{in} = 4; P_{out} = 2) − (P_{in} = 4; P_{out} = 4); (**d**) (P_{in} = 4; P_{out} = 0) − (P_{in} = 4; P_{out} = 2); (**e**) (P_{in} = 8; P_{out} = 6) − (P_{in} = 8; P_{out} = 8); (**f**) (P_{in} = 8; P_{out} = 4) − (P_{in} = 8; P_{out} = 6; (**g**) (P_{in} = 8; P_{out} = 2) − (P_{in} = 8; P_{out} = 4); (**h**) (P_{in} = 8; P_{out} = 0) − (P_{in} = 8; P_{out} = 2).

Realising that the aforementioned explanation needs further (quantitative) analyses, CO_2 concentration profiles in the axial direction have been drawn in Figure 8 for all the remaining cases from Table 2. It is noteworthy that these profiles do not show differences in CO_2 concentration, as was the case in Figure 7. Each graph in the figure is drawn in order to highlight the effect of outlet pressure on CO_2 concentration in the Opalinus Clay model. The solid line curves are the same as shown in Figure 6, for injection pressures of 2 MPa, 4 MPa, and 8 MPa. It can be seen in Figure 8a that increasing the outlet pressure to 1 MPa, which consequently results in a lower pressure gradient, leads to significantly lower CO_2 concentration in Opalinus Clay. While in the case of a 2 MPa pressure gradient, the lowest CO_2 concentration recorded was 85% at y = Y = 0.7, in the case of a 1 MPa pressure gradient, the lowest CO_2 concentration of 79% is observed at the outlet boundary. It is also noteworthy that with a reduced pressure gradient, the curve does not resemble the C-shape anymore; rather, a gradual decrease in CO_2 concentration is observed from y = Y = 0.05 to 1. The same trends are observed at injection pressures of 4 MPa and 8 MPa.

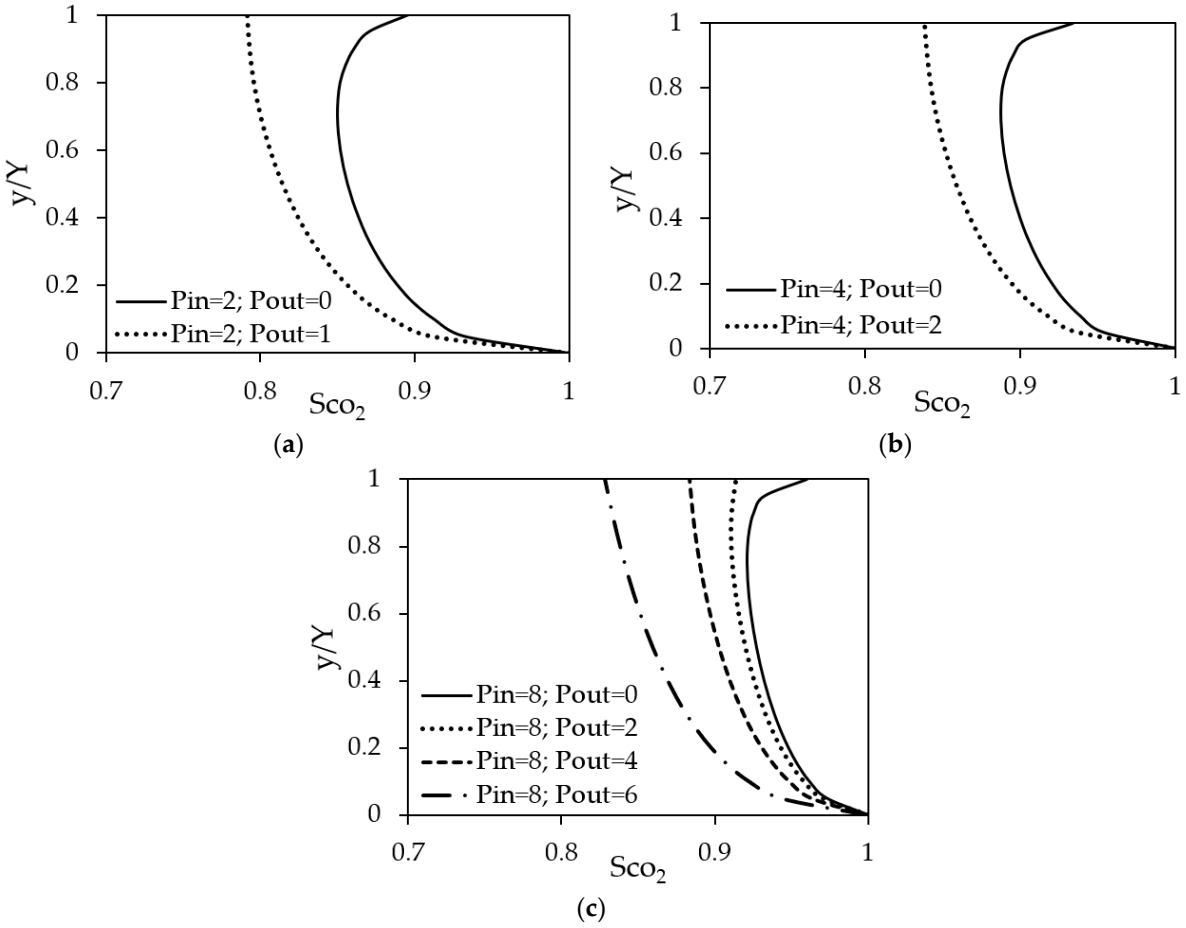

Figure 8. CO_2 concentration profiles in Opalinus Clay for different levels of pressure gradients: (**a**) P_{in} = 2 MPa; (**b**) P_{in} = 4 MPa; (**c**) P_{in} = 8 MPa.

5. Conclusions

The pressure gradient across caprocks plays an important role in CO_2 geosequestration. Numerical investigations have been carried out to evaluate the role of CO_2 injection pressure and the core (downstream) pressure towards local CO_2 concentration in the Opalinus Clay model. A coupled geomechanical and multiphase flow model based on CFD-FEM coupling, has been employed to gauge the complex nature of this phenomena. Detailed investigations and extensive quantitative analyses have revealed a number of interesting facts. Based on the results obtained, we conclude the following:

- Sub-critical CO_2 injection in Opalinus Clay for geosequestration is possible under the right conditions.
- Sub-critical CO_2 injection in Opalinus Clay under no pressure gradient leads to very low CO_2 concentration (maximum 5%).
- An increase in pressure gradient leads to higher CO_2 concentration in Opalinus Clay.
- An increase in outlet pressure results in lower CO_2 concentration in the model.
- For optimal sub-critical CO_2 geosequestration in Opalinus Clay, the injection pressure should be 8 MPa, and the outlet pressure should be minimum, ideally close to 0 MPa.

It is envisaged that the results of this study will aid in deciding the appropriateness of the geological formation for CCS projects, leading towards their technical feasibility and economic viability.

Author Contributions: H.K.H. contributed to conceptualization, data preparation, simulation, technical testing, writing, and interpretation. T.A., identified as the corresponding author, played a key role in the conceptualization, review, editing, feedback, supervision, model accuracy assessments, and writing. All authors have read and agreed to the published version of the manuscript.

Funding: The research received no external funding.

Data Availability Statement: Data is contained within the article.

Conflicts of Interest: The authors declare no conflicts of interest.

References

1. Rigby, S.P.; Alsayah, A.; Seely, R. Impact of Exposure to Supercritical Carbon Dioxide on Reservoir Caprocks and Inter-Layers during Sequestration. *Energies* **2022**, *15*, 7538. [CrossRef]
2. Allen, M.J.; Faulkner, D.R.; Worden, R.H.; Rice-Birchall, E.; Katirtsidis, N.; Utley, J.E.P. Geomechanical and petrographic assessment of a CO_2 storage site: Application to the Acorn CO_2 Storage Site, offshore United Kingdom. *Int. J. Greenh. Gas Control* **2020**, *94*, 102923. [CrossRef]
3. Raza, A.; Gholami, R.; Rezaee, R.; Rasouli, V.; Rabiei, M. Significant aspects of carbon capture and storage—A review. *Petroleum* **2019**, *5*, 335–340. [CrossRef]
4. Hawez, H.K.; Asim, T. Impact of Regional Pressure Dissipation on Carbon Capture and Storage Projects: A Comprehensive Review. *Energies* **2024**, *17*, 1889. [CrossRef]
5. Kim, S.; Hosseini, S.A. Study on the ratio of pore-pressure/stress changes during fluid injection and its implications for CO_2 geologic storage. *J. Pet. Sci. Eng.* **2017**, *149*, 138–150. [CrossRef]
6. Rahman, M.J.; Fawad, M.; Mondol, N.H. 3D Field-Scale Geomechanical Modeling of Potential CO2 Storage Site Smeaheia, Offshore Norway. *Energies* **2022**, *15*, 1407. [CrossRef]
7. Favero, V.; Laloui, L. Impact of CO_2 injection on the hydro-mechanical behaviour of a clay-rich caprock. *Int. J. Greenh. Gas Control* **2018**, *71*, 133–141. [CrossRef]
8. Song, Y.; Jun, S.; Na, Y.; Kim, K.; Jang, Y.; Wang, J. Geomechanical challenges during geological CO_2 storage: A review. *Chem. Eng. J.* **2023**, *456*, 140968. [CrossRef]
9. Hu, Q.; Wang, Q.; Zhang, T.; Zhao, C.; Iltaf, K.H.; Liu, S.; Fukatsu, Y. Petrophysical properties of representative geological rocks encountered in carbon storage and utilization. *Energy Rep.* **2023**, *9*, 3661–3682. [CrossRef]
10. Hawez, H.; Sanaee, R.; Faisal, N.H. Multiphase Flow Modelling in Fractured Reservoirs using a Novel Computational Fluid Dynamics Approach. In Proceedings of the 55th US Rock Mechanics/Geomechanics Symposium, Virtual, 18–25 June 2021.
11. Ladubec, C.; Gracie, R.; Craig, J. An extended finite element method model for carbon sequestration. *Int. J. Numer. Methods Eng.* **2015**, *102*, 316–331. [CrossRef]
12. Lesueur, M.; Rattez, H.; Zwarts, S.; Hajibeygi, H. Upscaling rocks mechanical properties to study Underground Hydrogen Storage feasibility. *Symp. Energy Geotech.* **2023**, *2023*, 2–3. [CrossRef]
13. Ismail, I.; Gaganis, V. Carbon Capture, Utilization, and Storage in Saline Aquifers: Subsurface Policies, Development Plans, Well Control Strategies and Optimization Approaches—A Review. *Clean Technol.* **2023**, *5*, 609–637. [CrossRef]
14. Mazzoldi, A.; Hill, T.; Colls, J.J. Assessing the risk for CO_2 transportation within CCS projects, CFD modelling. *Int. J. Greenh. Gas Control* **2011**, *5*, 816–825. [CrossRef]
15. Liu, X.; Asim, T.; Zhu, G.; Mishra, R. Theoretical and experimental investigations on the combustion characteristics of three components mixed municipal solid waste. *Fuel* **2020**, *267*, 117183. [CrossRef]
16. Vafaie, A.; Cama, J.; Soler, J.M.; Kivi, I.R.; Vilarrasa, V. Chemo-hydro-mechanical effects of CO_2 injection on reservoir and seal rocks: A review on laboratory experiments. *Renew. Sustain. Energy Rev.* **2023**, *178*, 113270. [CrossRef]

17. Singh, D.; Charlton, M.; Asim, T.; Mishra, R.; Townsend, A.; Blunt, L. Quantification of additive manufacturing induced variations in the global and local performance characteristics of a complex multi-stage control valve trim. *J. Pet. Sci. Eng.* **2020**, *190*, 107053. [CrossRef]
18. Cappa, F.; Guglielmi, Y.; Nussbaum, C.; De Barros, L.; Birkholzer, J. Fluid migration in low-permeability faults driven by decoupling of fault slip and opening. *Nat. Geosci.* **2022**, *15*, 747–751. [CrossRef]
19. Crisci, E.; Ferrari, A.; Giger, S.B.; Laloui, L. Hydro-mechanical behaviour of shallow Opalinus Clay shale. *Eng. Geol.* **2019**, *251*, 214–227. [CrossRef]
20. Liu, X.; Zhu, G.; Asim, T.; Zhang, Y.; Mishra, R. The innovative design of air caps for improving the thermal efficiency of CFB boilers. *Energy* **2021**, *221*, 119844. [CrossRef]
21. COMSOL. *Subsurface Flow Module User Guide, Version 6.0*; COMSOL: Burlington, MA, USA, 2022.
22. Chin, L.Y.; Raghavan, R.; Thomas, L.K. Fully Coupled Geomechanics and Fluid-Flow Analysis of Wells With Stress-Dependent Permeability. *SPE J.* **2000**, *5*, 32–45. [CrossRef]
23. Winhausen, L.; Khaledi, K.; Jalali, M.; Bretthauer, M.; Amann, F. The Anisotropic Behavior of a Clay Shale: Strength, Hydro-Mechanical Couplings and Failure Processes. *J. Geophys. Res. Solid Earth* **2023**, *128*, e2023JB027382. [CrossRef]
24. Sanaee, R.; Oluyemi, G.F.; Hossain, M.; Oyeneyin, M.B. Stress effects on flow partitioning in fractured reservoirs: Equivalent porous media versus poro-elasticity coupled modeling. In Proceedings of the 47th US Rock Mechanics/Geomechanics Symposium, San Francisco, CA, USA, 23–26 June 2013; American Rock Mechanics Association: San Francisco, CA, USA, 2013; Volume 3, pp. 2329–2337.
25. Bai, M.; Elsworth, D. Modeling of subsidence and stress-dependent hydraulic conductivity for intact and fractured porous media. *Rock Mech. Rock Eng.* **1994**, *27*, 209–234. [CrossRef]
26. Brooks, R.H.; Corey, A.T. Properties of Porous Media Affecting Fluid Flow. *J. Irrig. Drain. Div.* **1966**, *92*, 61–88. [CrossRef]
27. Minardi, A.; Stavropoulou, E.; Kim, T.; Ferrari, A.; Laloui, L. Experimental assessment of the hydro-mechanical behaviour of a shale caprock during CO_2 injection. *Int. J. Greenh. Gas Control* **2021**, *106*, 103225. [CrossRef]